LANGMUIR

Article

Cite This: Langmuir 2017, 33, 10374-10384

pubs.acs.org/Langmuir

Changes to DPPC Domain Structure in the Presence of Carbon Nanoparticles

Alan J. Sheridan,*[,†] Jonathan M. Slater,[†] Thomas Arnold,[‡] Richard A. Campbell,[§] and Katherine C. Thompson*[,†]

[†]Department of Biological Sciences and Institute of Structural and Molecular Biology, Birkbeck College, University of London, Malet Street, London WC1E 7HX, U.K.

[‡]I07, Diamond Light Source, Diamond House, Harwell Science & Innovation Campus, Didcot, Oxfordshire OX11 0DE, U.K.

[§]Institut Laue-Langevin, 71 avenue des Martyrs - CS 20156-38042, Grenoble 38000 Cedex 9, France

ABSTRACT: DPPC (dipalmitoylphosphatidylcholine) is a disaturated lipid capable of forming closely packed monolayers at the air−liquid interface of the lung and allows the surface tension within the alveoli to reduce to almost zero and thus prevent alveolar collapse. Carbon nanoparticles are formed in natural and man-made combustion events, including diesel engines, and are capable of reaching the alveolar epithelium during breathing. In this work, we have used Brewster angle microscopy and neutron reflectivity to study the effect of differing concentrations of carbon nanoparticles on the structure of DPPC monolayer as the monolayer is subject to compression and expansion. The results show that the inclusion of carbon nanoparticles within a DPPC monolayer affects the formation and structure of the lipid domains. The domains lose their circular structure and show a crenated structure as well as a reduction in overall size of the domains. This change in structure is also evident following expansion of the lipid monolayer, suggesting that some carbon nanoparticles may remain associated with the monolayer. This observation could have an important implication regarding the removal of nanosized airborne pollutants from the human lung.

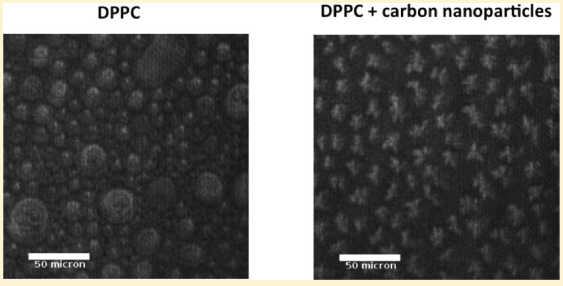

INTRODUCTION

The potential hazards of particulate pollutants, especially those produced in vehicle emissions, have recently seen a surge of interest in the media. Nanoparticles are defined as particles with a diameter of 100 nm or less, and carbonaceous nanoparticles are produced by combustion events, such as those in internal combustion engines. Recent emissions scandals involving major car manufacturers have heightened interest in this subject even more. Diesel engines emit particle matter in the range 6−62 nm.[1,2] Smaller nanoparticles in the range 6−11 nm are composed primarily of long-chained hydrocarbons, whereas particles in the range 52−62 nm are mostly carbonaceous, formed from the agglomeration of burnt lubricating oils and ash.[2] Kittelson et al. showed that a largest fraction of nanoparticles by number have a size distribution of <50 nm.[2] Research has shown a positive association between exposure to particles with an aerodynamic diameter of less than 2.5 μm ($PM_{2.5}$) led to an increase in hospital admission rates for respiratory conditions and cardiorespiratory mortality.[3,4] Epidemiological time series studies also indicate an adverse association between short-term exposure $PM_{2.5}$ and mortality and hospital admissions across a range of diseases and age groups.[5,6]

The air−liquid interface within the alveoli is one of the final lines of defense for the body from nanosized materials in the ambient air we breath. Clearly, with the increasing use of diesel-fueled vehicles, which are known producers of carbon particulates in the size ranges capable of reaching the deepest areas of the human lung, and increasing urbanization, resulting in greater exposure to these particulates, it is important that a systematic and detailed study of the effect of these particles on the behavior and functioning of the lung surfactant layer is studied.

Gas exchange in mammals takes place in the alveolar epithelium which represents up to 99% of the surface of the lung.[7] During inspiration, oxygen diffuses from the alveoli into the blood and carbon dioxide diffuses from the blood into the alveoli to be exhaled. The alveoli, being inside a mostly aqueous organism, have a layer of fluid on their internal surfaces. This fluid is called lung surfactant. One of the roles of the lung surfactant layer is to reduce the surface tension within the lungs to near zero when the internal area of the alveolus is at its minimum during expiration and thus prevent lung collapse.[8]

The lung surfactant itself is a mixture of lipid and protein with the proportions of lipid and proteins not varying greatly across the mammalian species.[9] The primary component of lung surfactant is lipid, which makes up to 90% by mass. The remaining 10% consists of the surfactant associated proteins SP-A, SP-B, SP-C, and SP-D.[7,9−11] Approximately 90% of the lipid consists of phospholipids and the remaining 10% consisting of neutral lipids, primarily cholesterol. Of the

Received: March 29, 2017
Revised: August 29, 2017
Published: September 20, 2017

DOI: 10.1021/acs.langmuir.7b01077
Langmuir 2017, 33, 10374−10384

phospholipid fraction, approximately 40% consists of the fully saturated dipalmitoylphosphatidylcholine (DPPC), making it the most abundant lipid in mammalian lung surfactant.

Nanoparticles are readily inhaled into the lungs, and their small aerodynamic diameter means that they have the potential to reach the lining of the alveoli and interact with the lung surfactant layer.[12,13] Several researchers have studied the effects of different categories of nanoparticle on both the lipid and protein components of surfactant.[14−18]

The surface pressure−area isotherm of a pure DPPC monolayer on an aqueous subphase will not usually show collapse until a surface pressure of approximately 70 mN m^{-1}.[19] The ability of the surfactant layer to avoid collapse at high surface pressures is important if it is to maintain its integrity during exhalation. Surface tension, which is directly related to surface pressure, must be as low as possible during exhalation if the alveoli are not to collapse. A reduction in the maximum surface pressure that can be achieved by the surfactant layer under compression corresponds to an increase in the surface tension. The inclusion of nanosized materials into the monolayers has been show to facilitate a reduction in the surface pressure maximum before collapse. The inclusion of 187 and 313 nm gelatin-based nanoparticles into a DPPC monolayer reduces its collapse pressure by approximately 10 mN m^{-1}.[14] The measure of a material's effect on the surface pressure, and consequently the surface tension of a liquid, is its surface activity. Surface activity of the pulmonary surfactant following exposure to aluminosilicate nanoparticles was measured with pulsating bubble surfactometry (PBS), which measures surface pressure during sinusoidal pulsations of an air bubble.[15] The authors observed that two of the aluminosilicate nanoparticle materials (Halloysite and Bentonite) caused a decrease in surface activity which they attributed to the adsorption of surfactant onto the nanoparticle surface, thus reducing the concentration of surfactant molecules in the liquid. The hydrophobic nanomaterial polyorganosiloxane (AmOrSil20) strongly associates with three-dimensional lipid/protein structures in the monolayer consisting of DPPC, the anionic lipid DPPG, and SP-C and that these interactions could affect the respreading of surfactant at the onset of the next inhalation cycle.[20] Also, Dwivedi et al. observed that 12 nm diameter polyorganosiloxane nanoparticles disrupt the domain morphology of the LE phase but show little change in phase transition, whereas larger nanoparticles of 136 nm diameter have the effect of expanding the surface pressure−area isotherm and causing a large disruption in domain structures.[21]

Guzmán et al. exposed DPPC monolayers on an aqueous subphase to carbon black nanoparticles with an average size of 15−29 nm. They found that that surface pressure−area isotherms were shifted to higher areas per DPPC molecule.[22] Also, the collapse pressure of the monolayer was reduced with increasing nanoparticle fraction. Brewster angle microscopy (BAM) images where recorded following the addition of high levels of carbon black nanoparticles (mole fractions of 0.33−0.75) to preformed DPPC monolayers at 7.5 mN m^{-1}. The results suggested low levels of aggregation of the hydrophobic carbon particles. Guzmán et al. also identified changes in the phase behavior and collapse parameters of a DPPC monolayer when exposed to hydrophobic fumed silica nanoparticles.[23]

Sosnowski et al. studied the effect of carbon particles (200 nm aggregates) and benzo-[*a*]-pyrene on a DPPC monolayer and found that the addition of carbon nanoparticles into the monolayer resulted in a reduction of the surface activity.[24] They suggested that this was due to the depletion of lipid due to adsorption onto the nanoparticles. Sosnowski et al. also observed similar lipid depletion effects on DPPC monolayers exposed to hydrophilic aluminosilicate nanoparticles.[25]

Carbon nanomaterials in the form of spherical fullerenes (C60, C180, C540, 5 × C60 nanostructures) were found to slightly increase surface tension in a DPPC monolayer with increasing concentration.[26] The authors suggest the inclusion of carbon nanoparticles into the DPPC monolayer, the formation of multiple small, particle filled bicelles during compression, and the formation of bilayer-like structures in the form of "buds" surrounding the carbon nanoparticles decrease the rigidity and order of the monolayer. The authors suggest that this results in the observed decrease in collapse pressure and a shift to higher area per molecule of the isotherm during compression.

Simulations of monolayers containing DPPC, dioleoylglycerophosphocholine (DOPC), and cholesterol exposed to C60 fullerene nanoparticles also showed an effect in the collapse pressure.[27] Without the presence of nanoparticles, the simulated monolayers collapse at a surface tension of around 0 mN m^{-1}. However, in the presence of the C60 nanoparticles the monolayer collapses at higher surface tensions (in the order of 10 mN m^{-1}). These results suggest that there is an interaction with one or more components of the lung surfactant system and nanoparticle materials.

Monolayers of pure DPPC spread at the air−water interface form well-defined, close-packed structures known as *domains*. Within the domains the molecules are in a ordered liquid-condensed (LC) phase surrounded by lipids in a liquid-expanded phase, (LE).[28] Other researchers have identified the presence of DPPC domains in lipid monolayers under compression, and the effect of hydrophilic silica nanoparticles on domain formation has been studied by Guzmán et al. where they found that the presence of silica nanoparticles resulted in nucleation at smaller areas per molecule in the LC phase, producing smaller domains.[29] Guzmán et al. also showed that silica nanoparticles in the range 9−60 nm prevented the formation of completely condensed phases in DPPC monolayers.[30] They identified small circular LC domains surrounded by LE phase even at high compression and that the LE phase was high in levels of silica nanoparticles, preventing domain growth and coalescence.

This study focuses on the effect of low levels of carbon nanoparticles on monolayers of the major lung surfactant lipid DPPC spread at the air−water interface, at relatively low surface pressures. Changes in the shapes of the surface pressure isotherms and the effects on the macroscopic lipid structure at the interface will be discussed.

EXPERIMENTAL METHODS

The nanoparticles used were commercially available carbon nanopowder (<50 nm particle size by TEM; Sigma-Aldrich, St. Louis, MO). The carbon nanoparticles were used without further purification. For SEM and AFM images, 0.1 mg of the carbon nanoparticles was dissolved in 1 mg mL^{-1} solution of DPPC in chloroform. Sizing of the nanoparticles was carried out using Gwiddion data analysis software. AFM (Dimension 3100 AFM, Bruker AFM Probes) and SEM (JSM 35 SEM, JEOL Ltd.) images of the carbon nanoparticles used are shown in Figures 1 and 2. The results show the average diameter of 156 nanoparticles to be 47.6 ± 0.2 nm.

DPPC was purchased from Avanti Polar Lipids (Alabaster, AL) and used without further purification. The lipid was dissolved in chloroform to a concentration of 1 mg mL^{-1}. Known quantities of the

DOI: 10.1021/acs.langmuir.7b01077
Langmuir 2017, 33, 10374−10384

carbon nanoparticles were weighed out and added to the lipid chloroform mixture to make lipid/nanoparticle mixtures of 0.1%−10.0% carbon nanoparticles to DPPC by mass. Monolayers of DPPC on an aqueous subphase were formed by depositing the DPPC in chloroform using a Hamilton syringe onto a subphase of pure water (Millipore Milli-Q, 18 MΩ cm) on the Langmuir−Blodgett trough (Nima Technologies, Coventry, UK).

Using the Langmuir−Blodgett trough, the surface of the subphase was compressed using movable barriers composed of Delrin (polyoxymethylene), thus reducing the area per molecule of the surface monolayer.

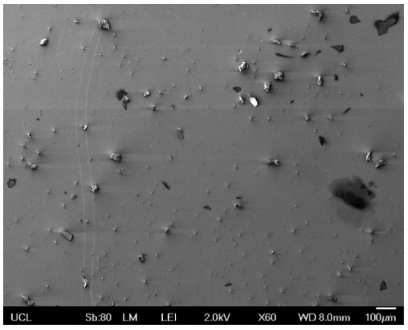

Figure 1. SEM image of carbon nanoparticles and DPPC prepared as described in the main text.

The surface pressure, π, of an interface is defined as the difference in surface tension of the interface when it has a layer of surfactant, γ, and the surface tension of the interface without surfactant, γ_0:

$$\pi = \gamma_0 - \gamma \quad (1)$$

where the units of π, γ_0, and γ are in mN m^{-1}.

The surface pressure was recorded as the area per molecule changed using a Wilhelmy plate (Whatman No. 1, Maidstone, UK).

By measuring the surface pressure of the air/water interface as a function of the monolayer area, the surface pressure/area isotherm can be obtained. It is this surface pressure/area isotherm that provides us with a measure of the phase changes that the monolayer undergoes under compression and expansion and the effect of the monolayer on the surface pressure of the subphase as a function of monolayer area.

BAM is an optical technique used for the study of thin layers of material on a solid or liquid surface and relies on the extent by which a beam of polarized light is reflected from a surface. The technique makes use of the fact that when a beam of p-polarized light is incident on an ideal surface, there will be no reflection if the angle of incidence is at the Brewster angle, Θ_B; i.e., the beam will be fully transmitted through the subphase, and there will be zero specular reflectivity.[31] The value of the Brewster angle is a function of the refractive indices of the two materials and is given by

$$\tan \Theta_B = \frac{n_2}{n_1} \quad (2)$$

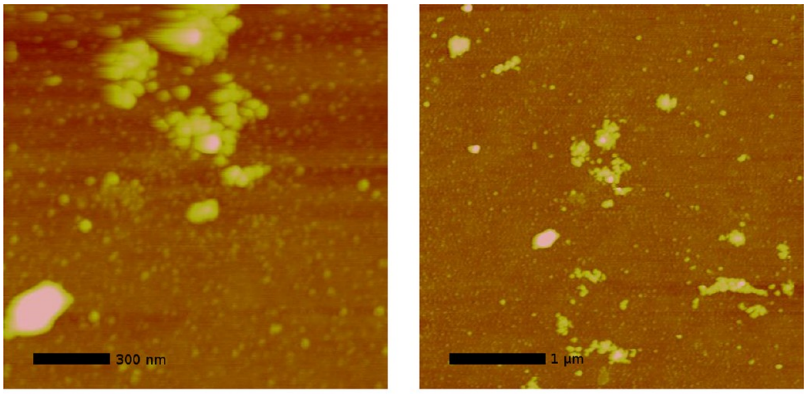

Figure 2. AFM images of carbon nanoparticles at (a) 1.5 μm and (b) 4 μm resolutions.

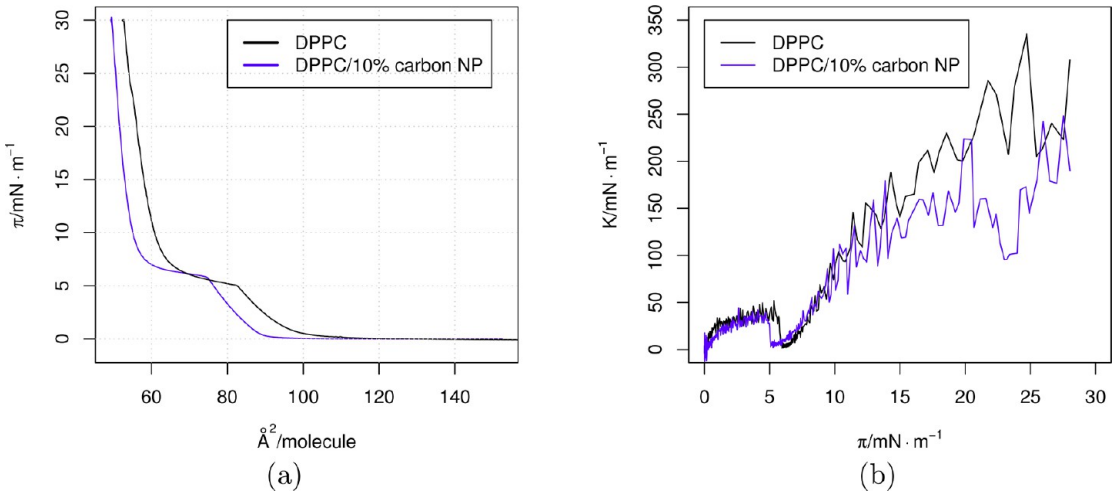

Figure 3. Surface pressure−area isotherms (a) and compression modulus plots (b) for DPPC monolayers as measured on a Langmuir−Blodgett trough. Isotherms were measured for pure DPPC and DPPC including 10.0% carbon nanoparticles to DPPC by mass. Isotherms were measured at 20 ± 1 °C.

DOI: 10.1021/acs.langmuir.7b01077
Langmuir 2017, 33, 10374−10384

where n_1 is the refractive index of the ambient material and n_2 is the refractive index of the subphase. In the case of the air−water interface, for visible light $n_1 \approx 1$ and for pure water $n_2 \approx 1.33$, giving $\Theta_B \approx 53°$. A beam of p-polarized light incident at an angle of 53° on an isotropic film present on a water subphase will be reflected if there is a difference in the refractive index between the film and the subphase.[32] The refractive index and reflectivity of a monolayer of DPPC on a water subphase depend upon the molecular packing, organization, and orientation (degree of anisotropy) of the DPPC.[32−34] For a monolayer of DPPC in the LE/LC region, the domains, where the DPPC molecules are closed packed with their palmitoyl chains aligned, will give substantially more reflectance than that for the disordered DPPC in the surrounding liquid expanded due to the anisotropy in the refractive index profile. Thus, BAM allows for the visualization of

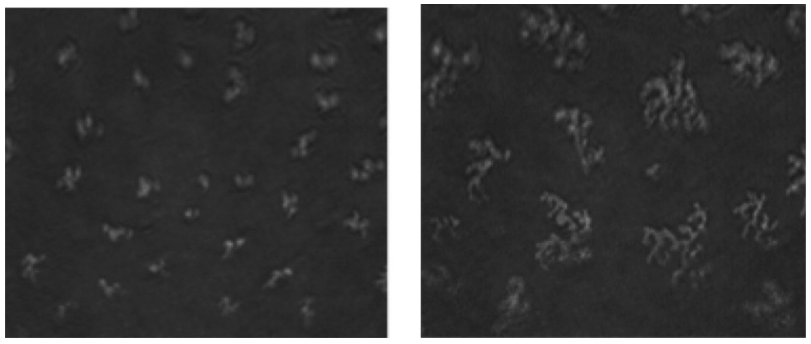

Figure 4. BAM image of DPPC monolayer spread at the air−water interface. Surface pressure was 3.7 and 4.3 mN m^{-1}.

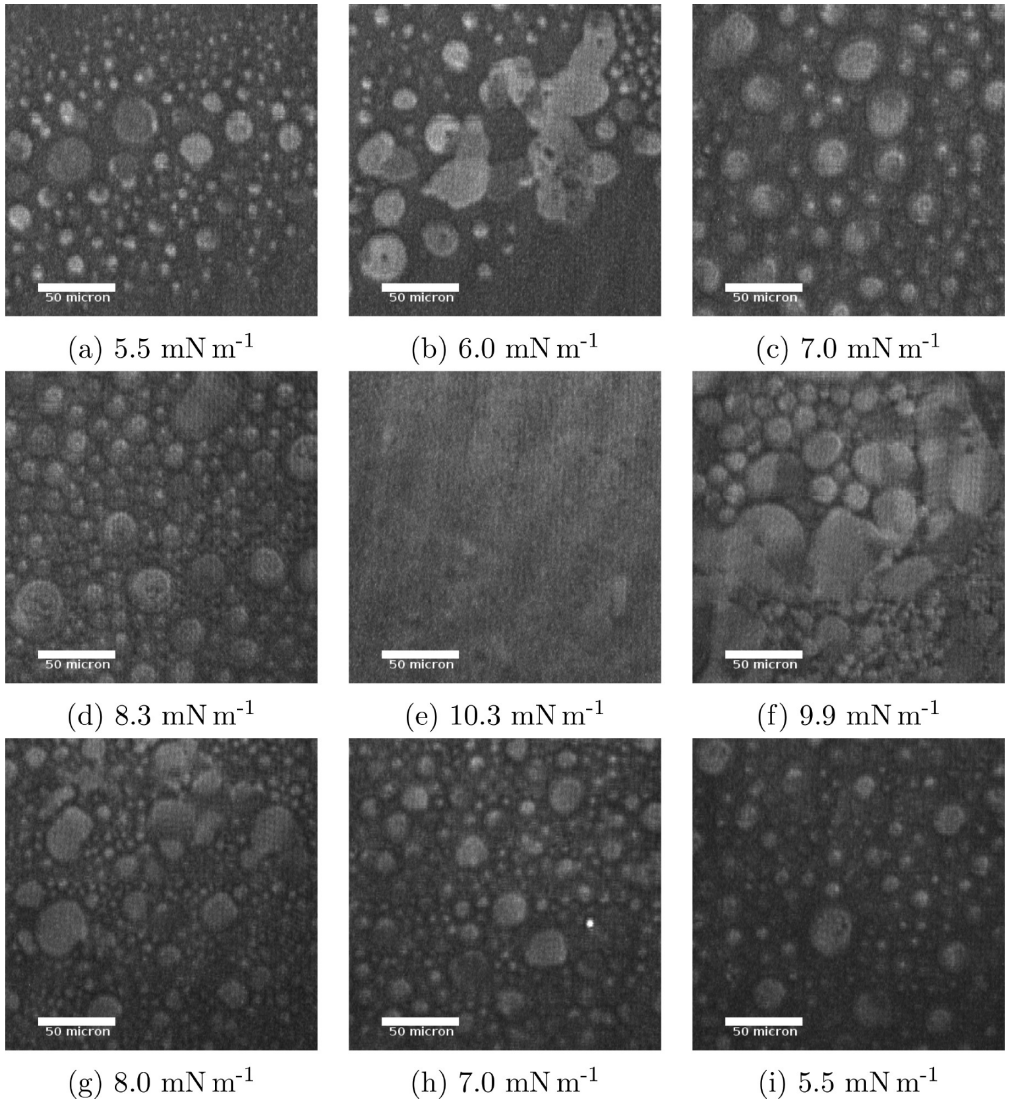

Figure 5. BAM images of DPPC on aqueous subphase. Images show liquid-condensed domains as surface pressure is increased from 5.5 mN m^{-1} by compression of the monolayer to a maximum of 10.3 mN m^{-1}, before expanding the monolayer again to a surface pressure of 5.5 mN m^{-1}. The liquid-condensed domains increase in size as the monolayer is compressed until a homogeneous monolayer is formed at 10.3 mN m^{-1}. The approximate areas per molecule are (a) 80, (b) 78, (c) 74, (d) 63, (e) 56, (f) 57, (g) 47, (h) 74, and (i) 80 $Å^2$/molecule.

DOI: 10.1021/acs.langmuir.7b01077
Langmuir 2017, 33, 10374−10384

domains of DPPC, as bright spots against a darker background. A particular benefit of BAM is that it allows for the visualization of the lipid domains without the need for fluorescent markers. The BAM system used was the Ellipsometry System EP^3 (Nanofilm Surface Analysis) at The Diamond Light Source, Harwell Science and Innovation Campus, Oxfordshire. The beam source was a p-polarized 50 mW laser (λ = 532 nm). For the BAM imagery, the images were taken with the Langmuir trough barriers stationary and with the temperature at 22 °C.

Neutron reflectivity of DPPC monolayers with and without 10% by mass carbon nanoparticles on an aqueous subphase was recorded using the FIGARO time-of-flight reflectometer at the Institut Laue-Langevin (Grenoble, France).[35] The monolayers were prepared on a Langmuir trough and held at constant pressures of 6.5 and 30 mN m^{-1} during the measurement. The incident beam with neutrons in a range of 2.2−25 Å was inclined at angles θ = 0.62° and θ = 3.79° to the interface. The reflectivity of the neutron flux was recorded as a function of the momentum transfer, q, normal to the surface, where $q = (4\pi/\lambda) \sin \theta$, and λ is the neutron wavelength. All reflectivity data were measured at a subphase temperature of 20 °C. Two different isotopic contrasts were employed: (1) regular DPPC, referred to as h62-DPPC, on a pure D_2O subphase and (2) a chain-deuterated form of DPPC, d62-DPPC, on a mixture of H_2O and D_2O, 92:8 v/v, which does not reflect neutrons and is termed "null reflecting water", as the subphase.

Data for the pure DPPC monolayers were fitted for each surface pressure using Motofit.[36] An interfacial two-layer model was used of neat chains and hydrated head groups. The principles used were as follows: (1) set the scattering length density of the chains layer to that calculated from their volume and scattering length (which depends just on the isotopic composition) with no air or solvent present; (2) set the three interlayer roughness values to that predicted by capillary wave theory; (3) set the scattering length density of the headgroup layer to that calculated for the volume of a headgroup and scattering length, with initially no solvent present, and adjust the thickness of the chains layer until the fit in contrast 2 is optimized; and (4) calculate the solvent volume fraction in the head groups layer to ensure physical reality of equal numbers of chains and heads in the monolayer with respect to different headgroup layer thicknesses until the fit in contrast 1 was optimized. As such, there were only two free fitting parameters. The scattering length density of the chains used was 0.36×10^{-6} Å^{-2} in contrast 1 and 6.87×10^{-6} Å^{-2} in contrast 2, from a volume of 892 Å^3 at 6.5 mN m^{-1} (allowing for the nonspecific interactions in the fluid phase).[37] The value used was -0.43×10^{-6} Å^{-2} in contrast 1 and 8.15×10^{-6} Å^{-2} in contrast 2, from a volume of 752 Å^3 at 30 mN m^{-1} (allowing for the specific

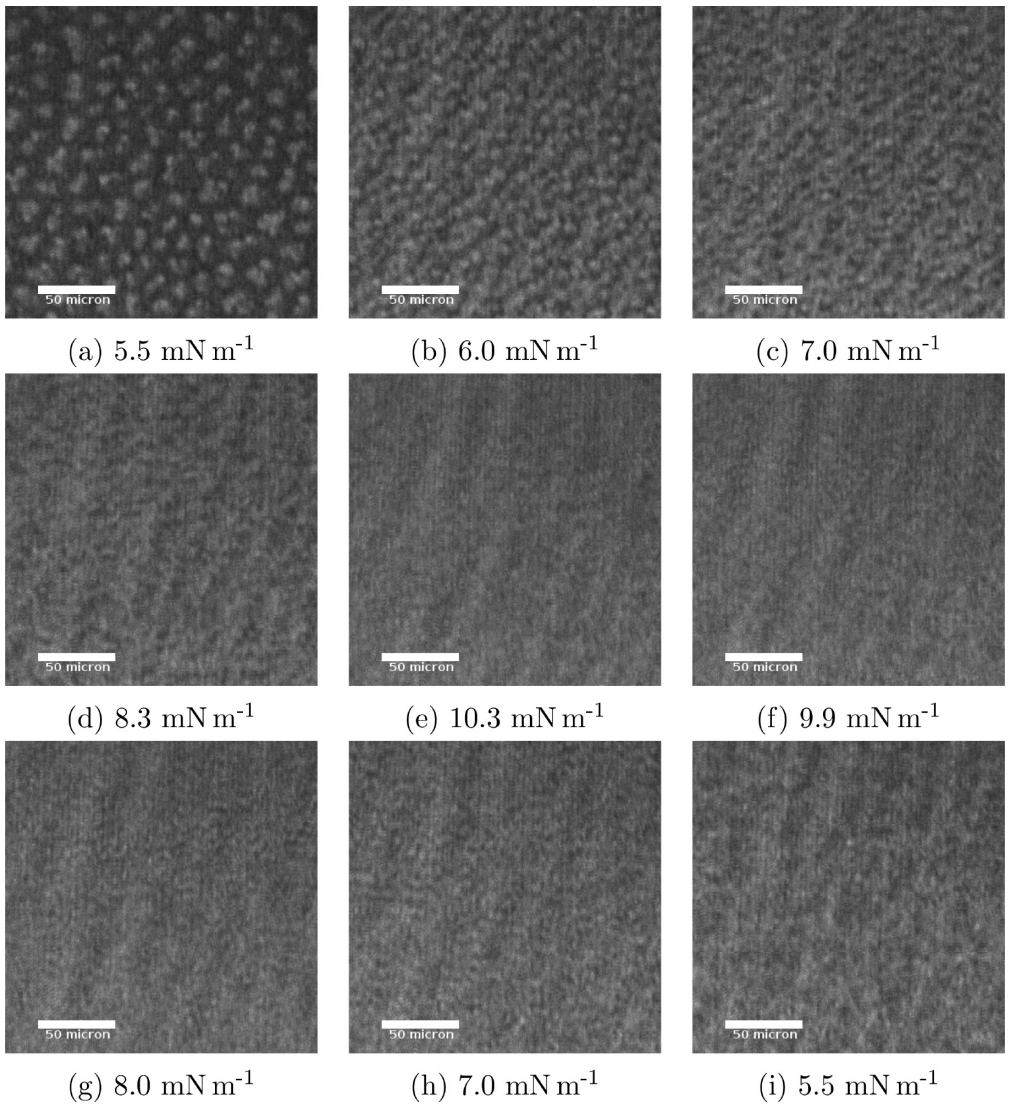

Figure 6. BAM images of 0.1% carbon nanoparticles to DPPC by mass on aqueous subphase. Images show liquid-condensed domains as surface pressure is increased from 5.5 mN m^{-1} by compression of the monolayer to a maximum of 10.3 mN m^{-1}, before expanding the monolayer again to a surface pressure of 5.5 mN m^{-1}. Small domain structures can still be observed at 10.3 mN m^{-1}.

DOI: 10.1021/acs.langmuir.7b01077
Langmuir 2017, 33, 10374−10384

interactions in the condensed phase).[37,38] The scattering length density of the heads used was 1.85×10^{-6} Å^{-2}. When the surface pressure was 6.5 mN m^{-1}, the chains layer had a thickness of 11.6 Å, the head groups layer had a thickness of 10 Å with 48% solvent, and the roughness values used were 3.0 Å. When the surface pressure was 30 mN m^{-1}, the chains layer had a thickness of 15.2 Å, the head groups layer had a thickness of 10 Å with 34% solvent, and the roughness values used were 3.5 Å. As is evident from the data presented in the Results section, there is no statistical difference in the model fits to the data with and without the nanoparticles, so a more elaborate model to incorporate the nanoparticles was not required.

RESULTS

Surface pressure−area isotherms for DPPC and DPPC with 10.0% by mass carbon nanoparticles are shown in Figure 3. If all the particles present in the 1% carbon particles to DPPC by mass solution resided at the interface, then these would occupy just ≈0.16% of the total area, similarly for the 10% by mass case, just 1.6% of the area would be taken up by the carbon particles, assuming a diameter of 50 nm.

At large areas, the DPPC isotherm shows a steady increase in surface pressure that indicates an increased packing of the lipid molecules in the homogeneous liquid-expanded (LE) phase. The isotherms of DPPC both with and without nanoparticles showed the characteristic plateau due to the coexistence of the fluid liquid-expanded (LE) phase and the ordered liquid-condensed phase (LC).[28,39] As the monolayer is compressed further, the surface pressure increases with a larger slope, indicating that only the LC phase is present. The DPPC/nanoparticle mixtures show a change in the slope of both the LC phase and the LC/LE coexistence phase, and plotting the surface compressional modulus, K, given by[40]

$$K = -A\left(\frac{\mathrm{d}\pi}{\mathrm{d}A}\right)_T \tag{3}$$

against surface pressure shows a reduction in the LC region (Figure 3b). The change in slope and reduction in surface compressional modulus can be explained as the incorporation of the carbon nanoparticles into the monolayer weakening the

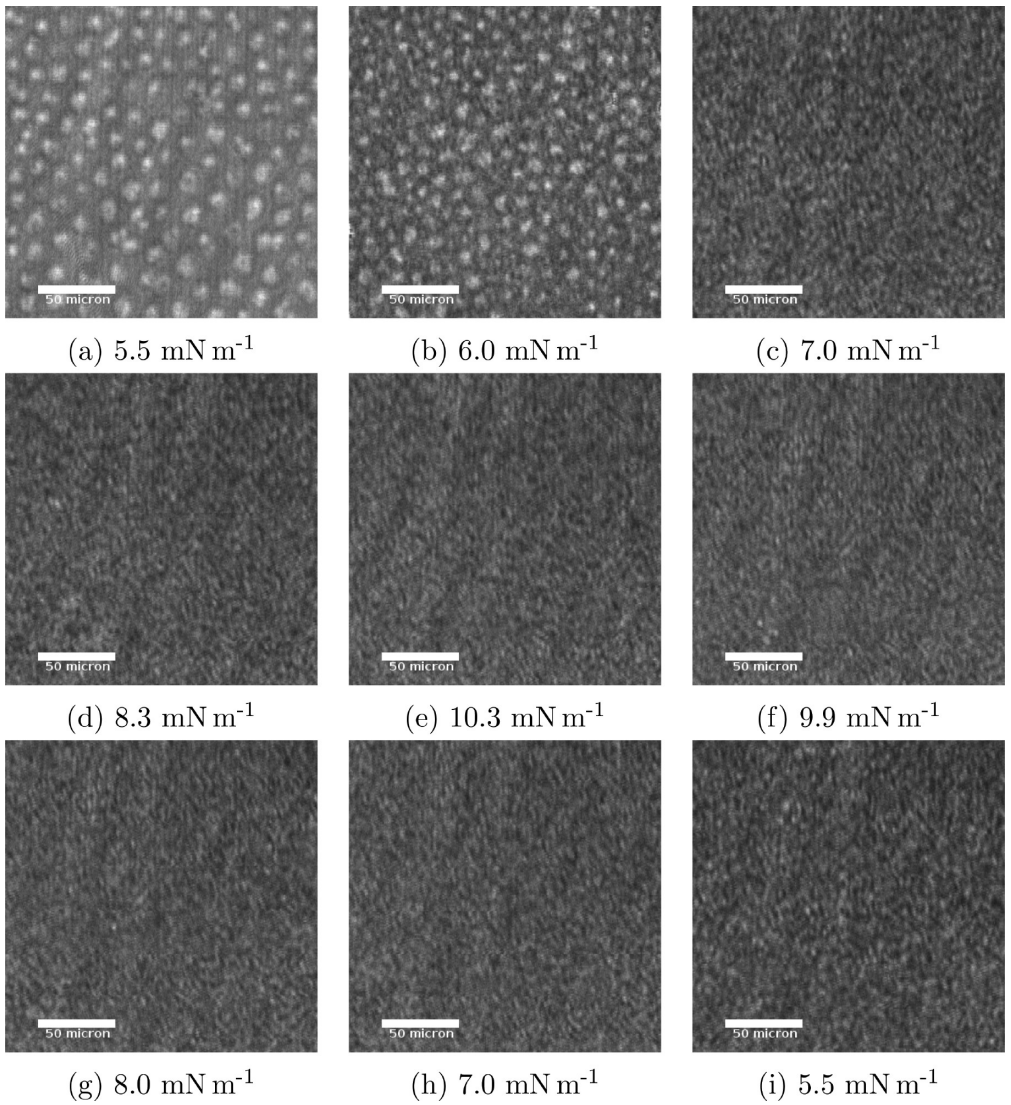

Figure 7. BAM images of 0.2% carbon nanoparticles to DPPC by mass on aqueous subphase. Images show liquid-condensed domains as surface pressure is increased from 5.5 mN m^{-1} by compression of the monolayer to a maximum of 10.3 mN m^{-1}, before expanding the monolayer again to a surface pressure of 5.5 mN m^{-1}. As with the case of the 0.1% carbon nanoparticles to DPPC by mass, there is a dominance of small, irregular domains.

DOI: 10.1021/acs.langmuir.7b01077
Langmuir 2017, 33, 10374−10384

cohesive interactions between the DPPC molecules at the interface.[29] This would result in a reduced packing density of the DPPC monolayer leading to the formation of the close-packed LC phase at smaller areas per molecule. The change in slope in the isotherm is also evident on expansion, and this would suggest that the nanoparticles are not expelled from the monolayer during the compression but remain associated with the lipid layer. This is consistent with the results shown by Brewster angle microscopy which shows that the morphological changes that affect domain formation are still evident on expansion of the monolayer.

Depositing the same amount of carbon nanoparticles alone to the air−water interface resulted in no increase in surface pressure when the trough area was compressed to the smallest value, and no features could be discerned on the BAM image.

BAM images of DPPC monolayers on a water subphase with varying amounts of carbon nanoparticles subjected to a compression and expansion cycle are presented in Figures 5−9. Parts (a) to (e) show the monolayer as it is compressed, and parts (f) to (i) show the monolayer during expansion.

BAM images of pure DPPC monolayers show the characteristic lobe shape at low surface pressures which begin to merge into approximately circular domains by 5.0 mN m^{-1} (Figure 4).

BAM images of pure DPPC monolayers (Figure 5) show the expected circular domains as described by other researchers.[28] As the monolayer is compressed, the domains merge to form a homogeneous monolayer at 10.3 mN m^{-1}. This surface pressure corresponds to the liquid-condensed (LC) phase of the monolayer isotherm. At this phase, the DPPC molecules are in a close-packed, ordered array. As the monolayer is re-expanded, the circular domains return. This corresponds to a return to the LC/LE plateau in the surface pressure−area isotherms as shown in Figure 3.

As has previously been observed for the interaction of hydrophobic silica nanoparticles with DPPC monolayers,[23] the inclusion of 0.1% carbon nanoparticles to DPPC by mass,

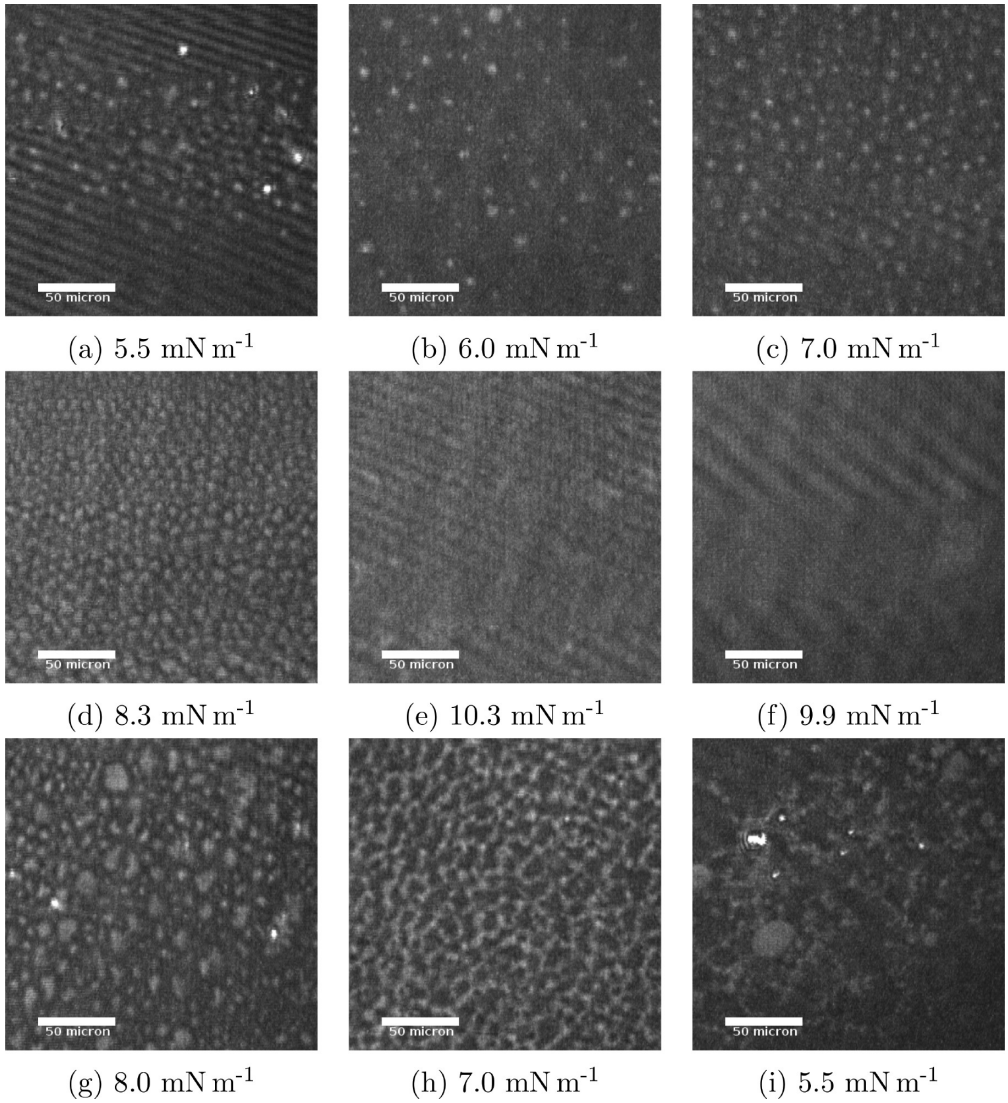

Figure 8. BAM images of 1.0% carbon nanoparticles to DPPC by mass on aqueous subphase. Images show liquid-condensed domains as surface pressure is increased from 5.5 mN m^{-1} by compression of the monolayer to a maximum of 10.3 mN m^{-1}, before expanding the monolayer again to a surface pressure of 5.5 mN m^{-1}. With the presence of the nanoparticles, the domains are smaller and more numerous than the domains observed with DPPC alone. During expansion, the lipid forms irregular, stringlike domains, and no reoccurrence of the large, round domains as seen with pure DPPC is observed.

DOI: 10.1021/acs.langmuir.7b01077
Langmuir 2017, 33, 10374−10384

there is evidence of a disruption in the formation of the lipid domains. The domains lose much of their regular, circular appearance. Also, the average size of the domains is reduced. A similar finding was previously noted by Guzmán et al. in their studies of silica nanoparticle interactions with DPPC monolayers.[30]

As the monolayer undergoes further compression, there appears to be an irregular structure to the monolayer. These results are also observed for the 0.2% carbon nanoparticles to DPPC by mass.

As the concentration of carbon nanoparticles is increased, small irregular domains are again observed. For the highest concentration of 10.0% carbon nanoparticles to DPPC by mass, the irregular domains take on a very distinctive crenelated structure as the pressure is increased.

The average sizes of the lipid domains shown in Figures 5−9 at 8.3 mN m^{-1} were measured. Sizing of the domains was carried using ImageJ 1.46. A plot of the results is shown in Figure 10. The plot shows a general trend of a reduction in the area for an increasing concentration of carbon nanoparticles, with an exception for the average area for the crenelated domains at the highest carbon nanoparticle concentration.

In response to the significant changes in the interfacial morphology induced by the presence of carbon nanoparticles in DPPC monolayers as demonstrated using BAM, we examined, using neutron reflectivity, if the interfacial structure of the lipid monolayer was significantly perturbed as a result. To maximize the detection of the technique to the presence of the carbon nanoparticles, measurements were carried out only at the maximum concentration of 10% particles by mass. In fact, if all the particles present in the mixture resided at the interface, then these would occupy just 1.6% of the total area, assuming a diameter of 50 nm. Figure 11 confirms that this very low surface coverage is below the detection limit because the reflectivity data with and without the nanoparticles at both surface pressures measured are statistically equivalent. Such

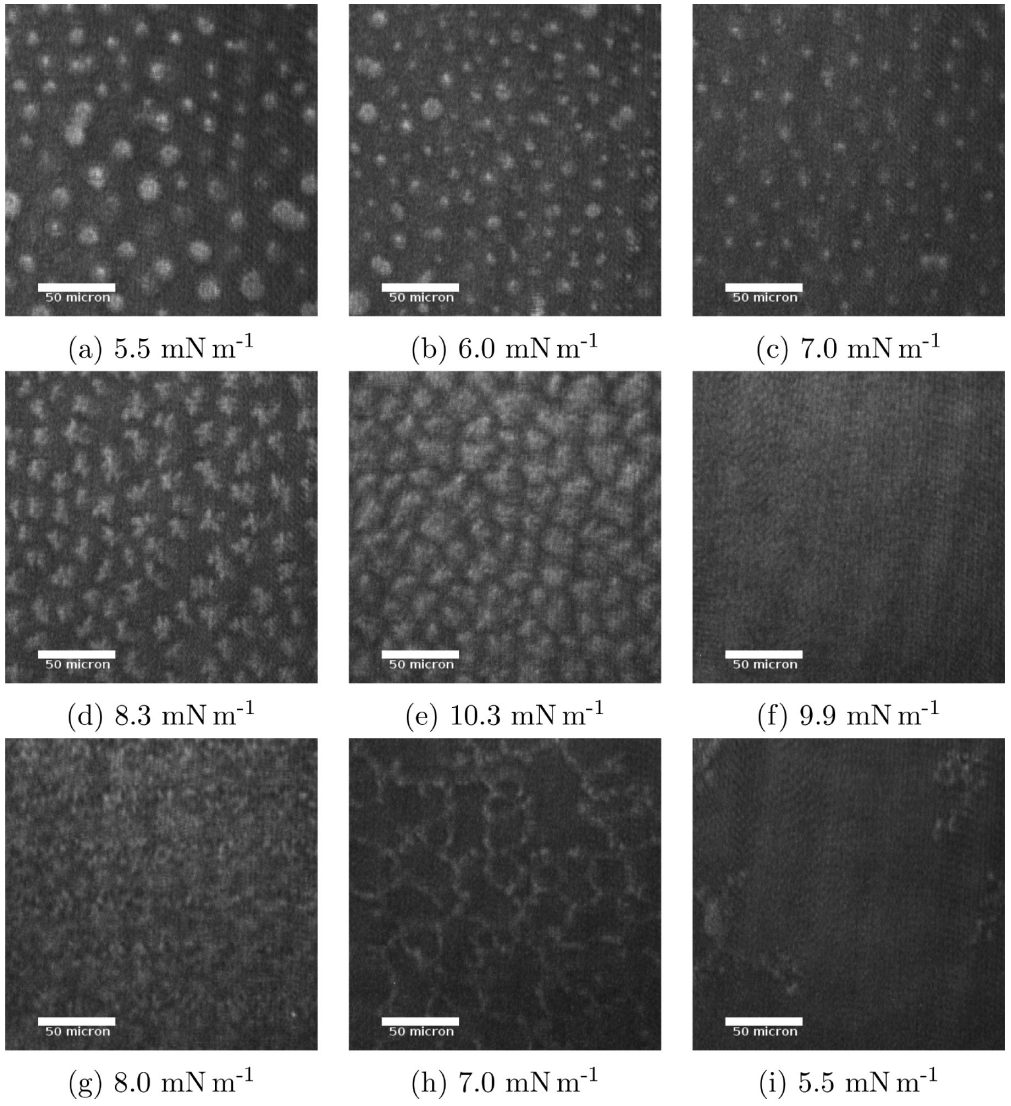

Figure 9. BAM images of 10.0% carbon nanoparticles to DPPC by mass on aqueous subphase. Images show liquid-condensed domains as surface pressure is increased from 5.5 mN m^{-1} by compression of the monolayer to a maximum of 10.3 mN m^{-1}, before expanding the monolayer again to a surface pressure of 5.5 mN m^{-1}. As is the case with the 1.0% carbon nanoparticles to DPPC by mass, the domains are smaller and more numerous than those formed by pure DPPC, and the stringlike lipid structures are again observed on expansion. The domains do not appear to reform at low surface pressure following compression. With this higher concentration of carbon nanoparticles, the domains take on an irregular, "crenelated" appearance at 8.3 and 10.3 mN m^{-1}.

DOI: 10.1021/acs.langmuir.7b01077
Langmuir 2017, 33, 10374−10384

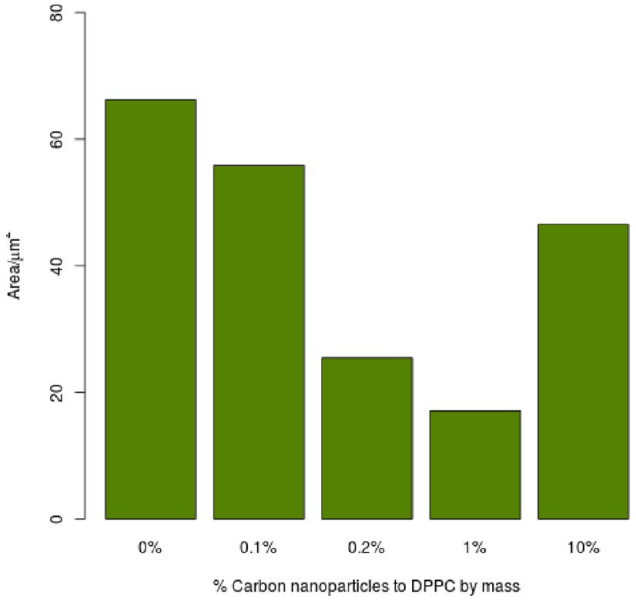

Figure 10. Plot of average sizes of DPPC domains on aqueous subphase as measured by BAM at 8.3 mN m^{-1}. The domain sizes were measured for DPPC with various concentrations of carbon nanoparticles. The average domains sizes for the concentrations of carbon nanoparticles were 66.2 μm^2 (0%), 55.9 μm^2 (0.1%), 25.5 μm^2 (0.2%), 17.1 μm^2 (1%), and 46.6 μm^2 (10%).

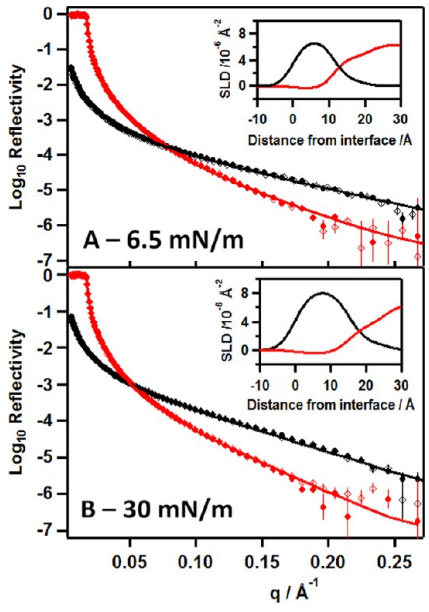

Figure 11. Neutron reflectivity of monolayers of pure DPPC (open diamonds) and DPPC with 10% by mass carbon nanoparticles (filled circles). The surface pressures was held at (A) 6.5 mN m^{-1} and (B) 30 mN m^{-1} during the measurements. The black data points are from d62-DPPC on a subphase of null reflecting water, and the red data points are from h62-DPPC on a subphase of D_2O.

pronounced changes in the lipid ordering and lateral morphology by the particles have no resulting effect on the measured mean lipid structure normal to the surface. At both surface pressures measured, the fitted lipid headgroup thickness remained the same at 10 Å, and the solvent fraction within the layer remained constant at the value required for physical matching of the density profiles of an equivalent number of chains and head groups.

DISCUSSION

The results show that the presence of carbon nanoparticles affects the formation of lipid domains in DPPC monolayers. At concentration as low as 0.1% carbon nanoparticles to DPPC molecules by mass, the domain structure of the monolayer is disrupted, resulting in smaller, irregular-shaped domains.

No previous studies are reported in the literature on the changes to domain formation for lipid monolayers at varying surface pressures in the presence of carbon nanoparticles at the sizes and low levels relevant to environmental concerns. The results are consistent with the work of Chakraborty et al.,[41] who studied the interaction of nanodiamond particles at slighty higher levels, and also Harishchandra et al., who reported that the presence of AmorSil20 nanoparticles, which, although of no environmental relevance, are also hydrophobic and showed disruption of DPPC lipid domains during compression.[42] Harishchandra et al. also used fluorescence imagery to show nanoparticle clusters aggregating at the edge of the lipid domains.

Carbon nanoparticles are hydrophobic. It would be reasonable to assume that in the presence of amphiphilic lipid and an aqueous solvent carbon nanoparticles would develop a "halo" of lipid molecules. The hydrophobic lipid tails would associate with the nanoparticle, while the polar heads would result in an increase in the hydrophilic character of the nanoparticle/lipid complex. If the coverage of the nanoparticle was complete, one could expect that lipid-coated nanoparticles would be able to leave the monolayer and migrate into the aqueous subphase. The Brewster angle microscopy results show similar disruption of the lipid domains upon both compression and expansion. This suggests that there is still a significant number of nanoparticles still associated with the monolayer and that they are still capable of disrupting domain formation in the monolayer upon expansion.

Notable from the BAM images of lipid domains is the smaller size of the domains within monolayers containing carbon nanoparticles. Also evident is the distinctive crenelated appearance of the domains at higher carbon nanoparticle concentrations.

A possible mechanism by which the presence of nanoparticles within a monolayer could affect domain growth is the formation of microscopic domains at first. The close-packed structure of these domains excludes nanoparticles. The domains would then grow as more DPPC molecules attach to the edges of the domains. The diffusion of the DPPC molecules into the domain would be hindered by the presence around the edges of the much larger nanoparticles. The aggregation of the nanoparticles around the perimeters of the lipid domains could therefore interfere with the coming together of smaller domains and hinder the formation of larger structures.

The changes in domain structure that are still seen during expansion indicate that the nanoparticles have remained associated with the lipid monolayer. If there is any expulsion of nanoparticles out of lipid monolayer due to lateral pressure during compression, this process appears to be reversible.

CONCLUSIONS

DPPC monolayers form distinctive ordered domains of close-packed molecules. Brewster angle microscopy shows that the inclusion of carbon nanoparticles in the DPPC monolayer at concentrations as low as 0.1% carbon nanoparticles to DPPC by mass results in smaller, more numerous domains than would be present in a DPPC monolayer without nanoparticles.

DOI: 10.1021/acs.langmuir.7b01077
Langmuir 2017, 33, 10374−10384

Also, as the concentration of nanoparticles is increased to 10.0% carbon nanoparticles to DPPC by mass, the lipid domains take on a crenelated appearance. It is possible that this is due to the presence of nanoparticle aggregates at the edge of growing domains inhibiting the free movement of lipid molecules onto the domain.

Although measurements with neutron reflectivity showed no change in the lipid structures as a result of the interaction with the nanoparticles, the Brewster angle microscopy images showed that the effects on domain size and shape were still present during re-expansion of the lipid monolayer. This suggests that the carbon nanoparticles remain associated with the lipid monolayer after compression.

Further study could be carried out to establish if repeated compression/expansion cycles were capable of expelling the nanoparticles from the lipid monolayer, which would be indicated by the reappearance of the domain morphology for pure DPPC.

This work shows that carbon nanoparticles with physical properties similar to those released by motor vehicle engines affect the organization of lung associated lipids. Although this study has only considered one of the components of mammalian lung surfactant, the results clearly indicate that exposure to carbon nanoparticles can significantly affect the organization and thus potentially the functioning on the lung surfactant system.

AUTHOR INFORMATION

Corresponding Authors

*E-mail: a.sheridan@mail.cryst.bbk.ac.uk (A.J.S.).
*E-mail: k.thompson@mail.cryst.bbk.ac.uk (K.C.T.).

ORCID

Thomas Arnold: 0000-0001-8295-3822
Richard A. Campbell: 0000-0002-6296-314X
Katherine C. Thompson: 0000-0002-9293-610X

Notes

The authors declare no competing financial interest.

ACKNOWLEDGMENTS

We express our gratitude to Steven Hudziak, Department of Electronic & Electrical Engineering, UCL, London, for recording the AFM images and Simon Wood, Institut Laue-Langevin, for technical support on FIGARO. We acknowledge the Institut Laue-Langevin for access to neutron beamtime on FIGARO (experiment number 70532) and Diamond Light Source for access to facilities associated with Beamline I07.

REFERENCES

(1) Kittelson, D. B. Engines and nanoparticles: a review. *J. Aerosol Sci.* **1998**, *29*, 575−588.

(2) Kittelson, D. B.; Watts, W. F.; Johnson, J. P. On-road and laboratory evaluation of combustion aerosols-Part 1: Summary of diesel engine results. *J. Aerosol Sci.* **2006**, *37*, 913−930.

(3) Dockery, D. W.; Pope, C. A.; Xu, X.; Spengler, J. D.; Ware, J. H.; Fay, M. E.; Ferris, B. G.; Speizer, F. E. An association between air pollution and mortality in six US cities. *N. Engl. J. Med.* **1993**, *329*, 1753−1759.

(4) Buckeridge, D. L.; Glazier, R.; Harvey, B. J.; Escobar, M.; Amrhein, C.; Frank, J. Effect of Motor Vehicle Emissions on Respiratory Health in an Urban Area. *Environ. Health Perspect.* **2002**, *110*, 293−300.

(5) Atkinson, R. W.; Kang, S.; Anderson, H. R.; Mills, I. C.; Walton, H. A. Epidemiological time series studies of PM2.5 and daily mortality and hospital admissions: a systematic review and meta-analysis. *Thorax* **2014**, *69*, 660−665.

(6) Brook, R. D.; Franklin, B.; Cascio, W.; Hong, Y. L.; Howard, G.; Lipsett, M.; Luepker, R.; Mittleman, M.; Samet, J.; Smith, S. C.; Tager, I. Air pollution and cardiovascular disease - A statement for healthcare professionals from the expert panel on population and prevention science of the American Heart Association. *Circulation* **2004**, *109*, 2655−2671.

(7) Goerke, J. Pulmonary surfactant: functions and molecular composition. *Biochim. Biophys. Acta, Mol. Basis Dis.* **1998**, *1408*, 79−89.

(8) Serrano, A. G.; Perez-Gil, J. Protein-lipid interactions and surface activity in the pulmonary surfactant system. *Chem. Phys. Lipids* **2006**, *141*, 105−118.

(9) Veldhuizen, R.; Nag, K.; Orgeig, S.; Possmayer, F. The role of lipids in pulmonary surfactant. *Biochim. Biophys. Acta, Mol. Basis Dis.* **1998**, *1408*, 90−108.

(10) Akella, A.; Deshpande, S. Pulmonary surfactants and their role in pathophysiology of lung disorders. *Indian J. Exp. Biol.* **2013**, *51*, 5−22.

(11) Parra, E.; Pérez-Gil, J. Composition, structure and mechanical properties define performance of pulmonary surfactant membranes and films. *Chem. Phys. Lipids* **2015**, *185*, 153−175.

(12) Muhlfeld, C.; Rothen-Rutishauser, B.; Blank, F.; Vanhecke, D.; Ochs, M.; Gehr, P. Interactions of nanoparticles with pulmonary structures and cellular responses. *Am. J. Physiol.* **2008**, *294*, L817−L829.

(13) Card, J. W.; Zeldin, D. C.; Bonner, J. C.; Nestmann, E. R. Pulmonary applications and toxicity of engineered nanoparticles. *Am. J. Physiol.* **2008**, *295*, L400−L411.

(14) Stuart, D.; Loebenberg, R.; Ku, T.; Azarmi, S.; Ely, L.; Roa, W.; Prenner, E. Biophysical Investigation of Nanoparticle Interactions with Lung Surfactant Model Systems. *J. Biomed. Nanotechnol.* **2006**, *2*, 245−252.

(15) Kondej, D.; Sosnowski, T. R. Alteration of biophysical activity of pulmonary surfactant by aluminosilicate nanoparticles. *Inhalation Toxicol.* **2013**, *25*, 77−83.

(16) Beck-Broichsitter, M.; Ruppert, C.; Schmehl, T.; Guenther, A.; Betz, T.; Bakowsky, U.; Seeger, W.; Kissel, T.; Gessler, T. Biophysical investigation of pulmonary surfactant surface properties upon contact with polymeric nanoparticles in vitro. *Nanomedicine* **2011**, *7*, 341−350.

(17) Beck-Broichsitter, M.; Ruppert, C.; Schmehl, T.; Guenther, A.; Seeger, W. Biophysical inhibition of synthetic vs. naturally-derived pulmonary surfactant preparations by polymeric nanoparticles. *Biochim. Biophys. Acta, Biomembr.* **2014**, *1838*, 474−481.

(18) Guzmán, E.; Liggieri, L.; Santini, E.; Ferrari, M.; Ravera, F. Effect of Hydrophilic and Hydrophobic Nanoparticles on the Surface Pressure Response of DPPC Monolayers. *J. Phys. Chem. C* **2011**, *115*, 21715−21722.

(19) Lee, K.; Yee, C. Collapse mechanisms of Langmuir monolayers. *Annu. Rev. Phys. Chem.* **2008**, *59*, 771−791.

(20) Sachan, A. K.; Harishchandra, R. K.; Bantz, C.; Maskos, M.; Reichelt, R.; Galla, H. J. High-Resolution Investigation of Nanoparticle Interaction with a Model Pulmonary Surfactant Monolayer. *ACS Nano* **2012**, *6*, 1677−1687.

(21) Dwivedi, M. V.; Harishchandra, R. K.; Koshkina, O.; Maskos, M.; Galla, H.-J. Size Influences the Effect of Hydrophobic Nanoparticles on Lung Surfactant Model Systems. *Biophys. J.* **2014**, *106*, 289−298.

(22) Guzmán, E.; Santini, E.; Zabiegaj, D.; Ferrari, M.; Liggieri, L.; Ravera, F. Interaction of Carbon Black Particles and Dipalmitoylphosphatidylcholine at the Water/Air Interface: Thermodynamics and Rheology. *J. Phys. Chem. C* **2015**, *119*, 26937−26947.

(23) Guzmán, E.; Santini, E.; Ferrari, M.; Liggieri, L.; Ravera, F. Interfacial Properties of Mixed DPPC-Hydrophobic Fumed Silica Nanoparticle Layers. *J. Phys. Chem. C* **2015**, *119*, 21024−21034.

(24) Sosnowski, T.; Kolinski, M.; Gradon, L. Interactions of Benzo-[*a*]-pyrene and Diesel Exhaust Particulate Matter with the

DOI: 10.1021/acs.langmuir.7b01077
Langmuir 2017, 33, 10374−10384

Lung Surfactant System. *Annals of occupational hygiene* **2011**, *55*, 329−338.
(25) Kondej, D.; Sosnowski, T. Effect of clay nanoparticles on model lung surfactant: a potential marker of hazard from nanoaerosol inhalation. *Environ. Sci. Pollut. Res.* **2016**, *23*, 4660−4669.
(26) Arick, D. Q.; Choi, Y. H.; Kim, H. C.; Won, Y. Y. Effects of nanoparticles on the mechanical functioning of the lung. *Adv. Colloid Interface Sci.* **2015**, *225*, 218−228.
(27) Barnoud, J.; Urbini, L.; Monticelli, L. C-60 fullerene promotes lung monolayer collapse. *J. R. Soc., Interface* **2015**, *12*, 20140931.
(28) Klopfer, K. J.; Vanderlick, T. K. Isotherms of dipalmitoylphosphatidylcholine (DPPC) monolayers: features revealed and features obscured. *J. Colloid Interface Sci.* **1996**, *182*, 220−229.
(29) Guzmán, E.; Liggieri, L.; Santini, E.; Ferrari, M.; Ravera, F. Influence of silica nanoparticles on thermodynamic and structural properties of DPPC-palmitic acid Langmuir monolayers. *Colloids Surf., A* **2012**, *413*, 280−287.
(30) Guzmán, E.; Orsi, D.; Cristofolini, L.; Liggieri, L.; Ravera, F. Two-Dimensional DPPC Based Emulsion-like Structures Stabilized by Silica Nanoparticles. *Langmuir* **2014**, *30*, 11504−11512.
(31) Honig, D.; Mobius, D. Reflectometry at the brewster-angle and brewster-angle microscopy at the air-water-interface. *Thin Solid Films* **1992**, *210-211*, 64−68.
(32) Hoenig, D.; Moebius, D. Direct visualization of monolayers at the air-water interface by Brewster angle microscopy. *J. Phys. Chem.* **1991**, *95*, 4590−4592.
(33) Overbeck, G. A.; Honig, D.; Mobius, D. Stars, stripes and shells in monolayers - simulation of the molecular arrangement in schlieren structures. *Thin Solid Films* **1994**, *242*, 213−219.
(34) Weidemann, G.; Gehlert, U.; Vollhardt, D. Inner structure of condensed-phase domains in monolayers at the air-water-interface. *Langmuir* **1995**, *11*, 864−871.
(35) Campbell, R. A.; Wacklin, H. P.; Sutton, I.; Cubitt, R.; Fragneto, G. FIGARO: The new horizontal neutron reflectometer at the ILL. *Eur. Phys. J. Plus* **2011**, *126*, 107.
(36) Nelson, A. Co-refinement of multiple-contrast neutron/X-ray reflectivity data using MOTOFIT. *J. Appl. Crystallogr.* **2006**, *39*, 273−276.
(37) Armen, R. S.; Uitto, O. D.; Feller, S. E. Phospholipid component volumes: Determination and application to bilayer structure calculations. *Biophys. J.* **1998**, *75*, 734−744.
(38) Small, D. M. Lateral chain packing in lipids and membranes. *J. Lipid Res.* **1984**, *25*, 1490−1500.
(39) Mingotaud, A. F.; Mingotaud, C.; Patterson, L. K. *Handbook of Monolayers*; Academic Press, Inc.: 1993; Vol. *1*.
(40) Vollhardt, D.; Fainerman, V. In *Interfacial Rheology*; Miller, R., Liggieri, L., Eds.; CRC Press: 2009; New aspects in the consideration of compressibility for the characterization of Langmuir monolayers.
(41) Chakraborty, A.; Mucci, N.; Tan, M.; Steckley, A.; Zhang, T.; Forrest, M.; Dhar, P. Phospholipid Composition Modulates Carbon Nanodiamond-Induced Alterations in Phospholipid Domain Formation. *Langmuir* **2015**, *31*, 5093−5104.
(42) Harishchandra, R. K.; Saleem, M.; Galla, H. J. Nanoparticle interaction with model lung surfactant monolayers. *J. R. Soc., Interface* **2010**, *7*, S15−S26.

DOI: 10.1021/acs.langmuir.7b01077
Langmuir 2017, 33, 10374−10384